AD-A119 632 COLD REGIONS RESEARCH AND ENGINEERING LAB HANOVER NH F/G 8/12
ACOUSTIC EMISSIONS FROM POLYCRYSTALLINE ICE,(U)
AUG 82 W F ST. LAWRENCE, D M COLE
UNCLASSIFIED CRREL-82-21 NL

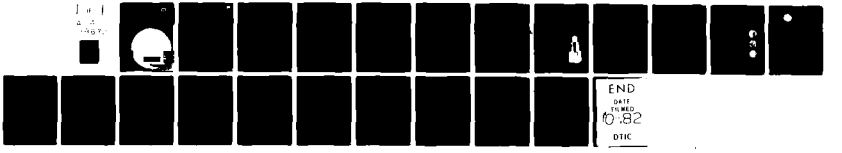

END
DATE FILMED
10-82
DTIC

CRREL REPORT 82-21

US Army Corps of Engineers
Cold Regions Research & Engineering Laboratory

Acoustic emissions from polycrystalline ice

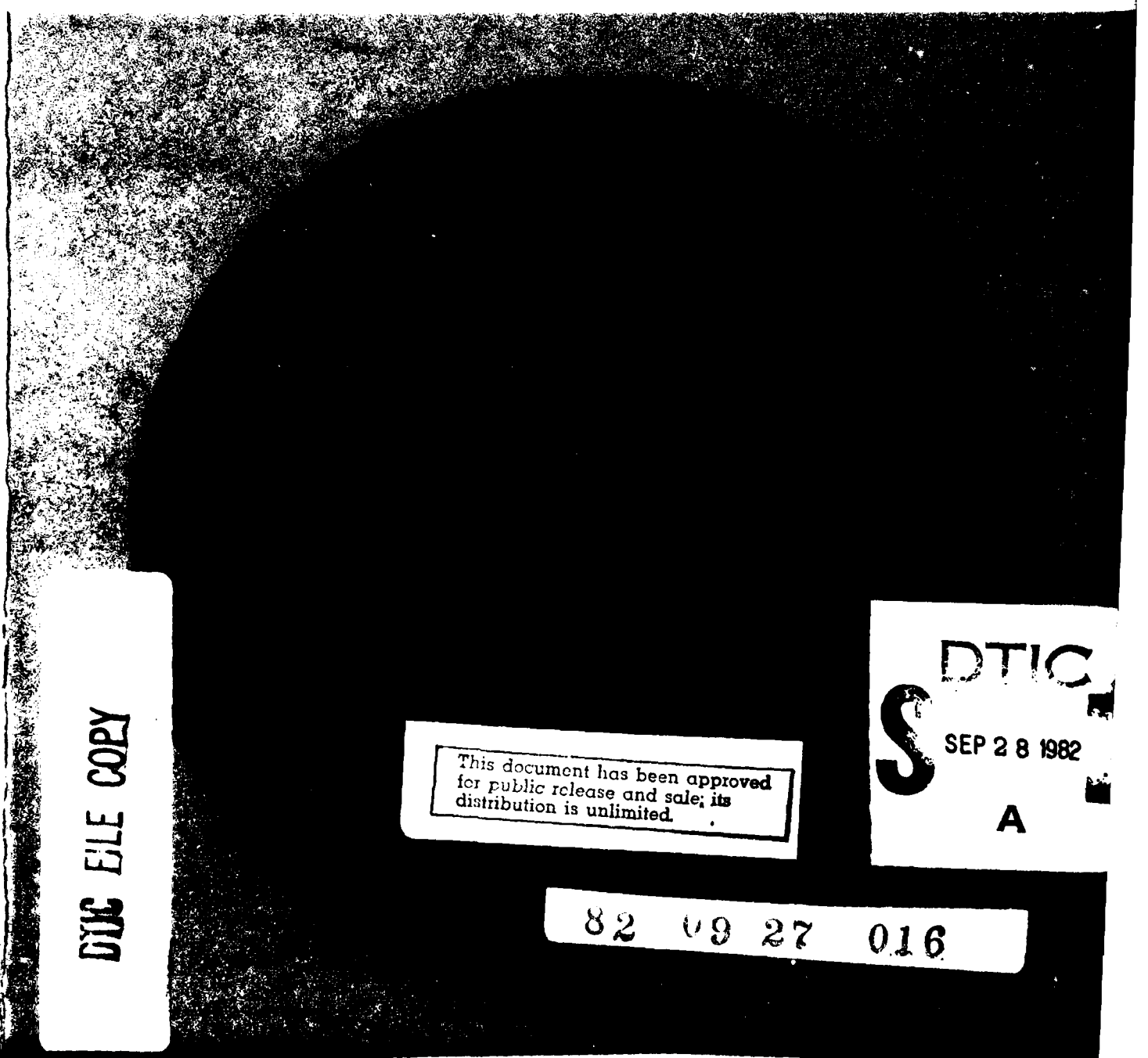

CRREL Report 82-21

August 1982

Acoustic emissions from polycrystalline ice

William F. St. Lawrence and David M. Cole

REPORT DOCUMENTATION PAGE

READ INSTRUCTIONS BEFORE COMPLETING FORM

1. REPORT NUMBER: CRREL Report 82-21	2. GOVT ACCESSION NO.: AD-A119632
3. RECIPIENT'S CATALOG NUMBER	
4. TITLE (and Subtitle): ACOUSTIC EMISSIONS FROM POLYCRYSTALLINE ICE	5. TYPE OF REPORT & PERIOD COVERED
	6. PERFORMING ORG. REPORT NUMBER
7. AUTHOR(s): William F. St. Lawrence and David M. Cole	8. CONTRACT OR GRANT NUMBER(s)
9. PERFORMING ORGANIZATION NAME AND ADDRESS: U.S. Army Cold Regions Research and Engineering Laboratory, Hanover, New Hampshire 03755	10. PROGRAM ELEMENT, PROJECT, TASK AREA & WORK UNIT NUMBERS: DA Project 4A161101A91D, Work Unit 336
11. CONTROLLING OFFICE NAME AND ADDRESS: U.S. Army Cold Regions Research and Engineering Laboratory, Hanover, New Hampshire 03755	12. REPORT DATE: August 1982
	13. NUMBER OF PAGES: 26
14. MONITORING AGENCY NAME & ADDRESS(if different from Controlling Office)	15. SECURITY CLASS. (of this report): Unclassified
	15a. DECLASSIFICATION/DOWNGRADING SCHEDULE

16. DISTRIBUTION STATEMENT (of this Report)

Approved for public release; distribution unlimited.

17. DISTRIBUTION STATEMENT (of the abstract entered in Block 20, if different from Report)

18. SUPPLEMENTARY NOTES

19. KEY WORDS (Continue on reverse side if necessary and identify by block number)

Acoustic emissions
Ice
Mechanical properties
Polycrystalline ice

20. ABSTRACT (Continue on reverse side if necessary and identify by block number)

The acoustic emission response from fine-grained polycrystalline ice subjected to constant compressive loads was examined. A number of tests were conducted with the nominal stress ranging from 0.8 to 3.67 MPa at a temperature of -5°C. The acoustic emission response was recorded and the data are presented with respect to time and strain. The source of acoustic emissions in ice is considered in terms of the formation of both microfractures and visible fractures that develop without catastrophic failure of the ice. A model to describe the acoustic emission response is developed.

PREFACE

This report was prepared by Dr. William F. St. Lawrence, Geophysicist, of the Snow and Ice Branch, Research Division, and David M. Cole, Research Civil Engineer, of the Applied Research Branch, Experimental Engineering Division, U.S. Army Cold Regions Research and Engineering Laboratory. Funding for this research was provided by DA Project 4A161101A91D, *In-House Laboratory Independent Research*, Work Unit 336, *Acoustic Emissions from Ice.*

Dr. Samuel Colbeck and Dr. Devinder Sodhi of CRREL technically reviewed the manuscript of this report.

The authors gratefully acknowledge the assistance of Barbara Hutching in the data reduction phase of this work.

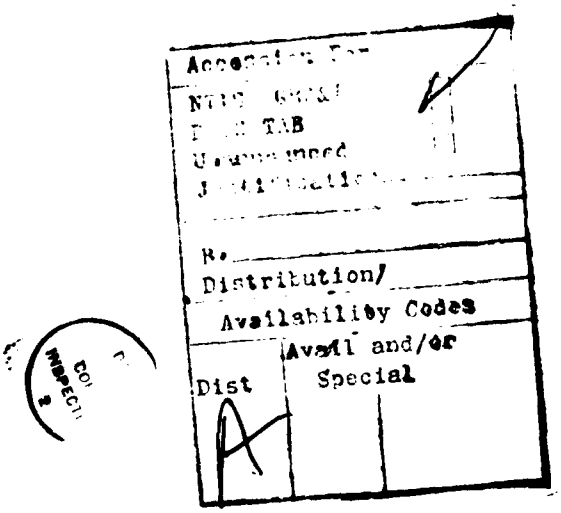

CONTENTS

ILLUSTRATIONS

TABLES

ACOUSTIC EMISSIONS FROM POLYCRYSTALLINE ICE

William F. St. Lawrence and David M. Cole

INTRODUCTION

A program has been underway to study the mechanical behavior of fine-grained polycrystalline ice subjected to mechanical loads. As part of this program we have monitored the acoustic emission activity associated with a number of uniaxial compression tests on ice samples subjected to constant loads. In this report we present the results of our research and discuss possible relationships between acoustic signals emitted from ice and its flow and fracture.

To the best of our knowledge no previous research has been conducted on the acoustic emissions from fine-grained equiaxed polycrystalline ice. Columnar grained ice has been used in acoustic emission research but it is highly anisotropic, whereas fine-grained ice tends to behave isotropically in the aggregate. Nevertheless, we have found that the acoustic emission response and development of internal fractures are qualitatively similar in both columnar grained ice and the fine-grained equiaxed ice tested here.

We have found the acoustic emission activity in ice to be a well-behaved function of stress under a variety of loading conditions at constant temperature and grain size. The results from a series of constant load creep tests are presented here.

BACKGROUND

Gold (1960) cites a paper by E. Brown (1926) who noted the presence of audible "crackling" of ice samples subjected to compressive loads. Brown associated this sound with the development of cracks in the ice. He also noted that the crackling of the ice was related to the level of the stress applied and the temperature at which the test was conducted

In his own research, Gold (1960) used a piezoelectric crystal frozen to his ice sample to monitor the fractures which took place in the ice. Gold's work most likely represents the first time that modern acoustic emission techniques were used to study ice. Gold reported that a signal was recorded each time a disturbance (fracture) took place in the ice.

Working at -10°C with ice subjected to uniaxial compressive loads, Gold was able to observe the stress limits for which his ice samples exhibited either decelerating or accelerating creep and also the stress limit at which cracking occurred. He found that the strain rate decreased for stresses below 1.57 MPa while above this value it exhibited a tertiary, or accelerating, stage. Gold also found that few cracks were observed for ice subjected to stresses below 0.98 MPa, that an appreciable number of cracks were detected at stresses of 1.4 MPa, and that the amount of cracking was greatly increased at the stress levels causing tertiary creep. Gold tested his ice samples with the long axis of the ice grains perpendicular to the applied load.

As Gold's research proceeded, he gave up his acoustical fracture detection method in favor of actually counting the visible fractures that occurred in each of his ice samples. This technique avoids the problem of recording, as separate events, the multiple acoustic signals that might emanate from the same fracture, but it does not permit the detection of microfractures or the examination of crack extension. Gold's research on the fracture of columnar grained ice, while only partially using acoustic emission monitoring techniques, is very germane to acoustic emission studies. Two particularly important papers on this work were

published by Gold in 1970 and 1972. Indeed much of the extensive Soviet literature on acoustic emissions in ice relies to a great extent on Gold's work.

The Soviet laboratory work, like Gold's, has concentrated on the acoustic activity associated with columnar grained ice subjected to constant loads under uniaxial compression. The Soviets have directed their effort toward incorporating the observed acoustic emission activity into a constitutive relationship for columnar grained ice.

Zaretsky et al. (1976) published a reasonably comprehensive paper regarding acoustic emissions and the deformation of ice. In this paper they indicate that the transducer used was piezoelectric in nature but do not state the frequency range over which they worked or the method they used to process the resulting signals. From personal communication with A. Fish, one of the Soviet paper's coauthors, we found that they generally worked in the audible region of the spectrum and used event-counting methods. Counting the number of cycles per event (ring down count) is common in many acoustic emission investigations in the West.

Zaretsky et al. (1976) note that the ice they tested showed marked dilatational effects, which are attributed to the introduction of fractures in the samples. They also report that each acoustic pulse corresponded to the formation of a single fracture or microcrack. They consider the amplitude of the pulse to be a characteristic of the size of the fracture generating it and the square of the amplitude to be proportional to the energy dissipated. A constitutive relationship is presented for the flow of ice under uniaxial compressive loads. This equation shows that the strain rate is proportional to the applied stress and also to the acoustic emission activity, while it is inversely proportional to time raised to a constant power.

Other Soviet research is reported by Gavrilo et al. (1979), who propose that tertiary creep results from the breakdown of intergranular bonds by microfracture. In this work, a limit stress σ_∞ coincides with the onset of tertiary creep. This appears to confirm Gold's (1972a and b) observations that at some critical crack density the onset of structural instability (tertiary creep) takes place.

In a recent Soviet paper on the deformation of ice (Zaretsky et al. 1979), a comprehensive theory of ice deformation is presented which incorporates the acoustic emission concepts given in their previous work. In this paper, the value of 0.5 MPa is determined to be the limit stress (σ_∞). The dimensions of the microfractures recorded by acoustic techniques are considered and a new flow relationship which incorporates both the acoustic emission amplitude and the number of events per unit volume is presented. A detailed analysis of the surface area of fractures is also given.

EXPERIMENTAL PROCEDURES

Ice specimens

The ice samples used for our work were prepared, as described by Cole (1979), from distilled de-aired water introduced into a mold containing sieved snow crystals. The specimens had a mean grain diameter of 1.2 mm and a density of 0.917 Mg m^{-3}. The c-axis of the ice crystals appeared to be randomly oriented. Some fine air bubbles with an average diameter of 0.1 mm appeared in the center of the samples. Generally, gas bubbles represented a very small volume fraction of the ice sample.

During the sample molding process, fabric-based phenolic end caps were frozen onto each specimen to provide a means for interfacing the sample with the test machines. The ice bonded intimately to the roughened surface of the end cap, and the difference in the thermal expansion coefficients of the materials

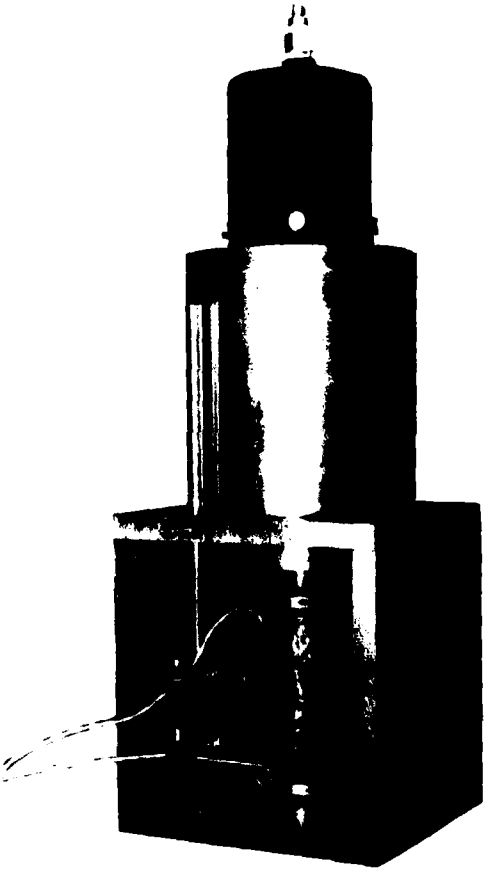

Figure 1. Ice specimen and alignment fixture.

was not great enough to cause excessive strains during gradual temperature changes. Also, displacement compatibility between cap and specimen was ensured and stress concentrations were avoided. We did not detect excessive fracturing of the ice in the vicinity of the end caps. In fact, we found that the visible fracture density in the vicinity of the end caps was generally lower than that found in the sample center.

The ice specimens were right circular cylinders, 127 mm long and 25.4 mm in radius. The resulting volume of each sample was 2.574×10^{-4} m^3. The end caps were of the same radius as the sample and 18 mm thick.

In all tests, each ice sample was covered with a thin latex membrane that prevented loss of mass due to sublimation. The specimen end caps were bolted to the base and the piston of a special jig for testing. The upper section of the apparatus, containing an air-actuated cylinder used for constant load tests, can be removed to allow for constant strain rate loading in a conventional testing machine. Thus, specimens were always mounted in the same fixture regardless of the type of test being performed. The ice specimen and alignment fixture with the acoustic emission transducers in place are shown in Figure 1.

Mechanical test equipment

The constant load experiments were generally conducted with a pneumatic ram attached to the test fixture. For high load tests (nominal stress greater than 2.5 MPa) an 89-kN capacity machine by Materials Test Systems was used. In the creep tests, loads were applied at the rate of 70 kPa s^{-1} until full load was reached when the pneumatic ram was used, and loads were applied at 1.0 MPa s^{-1} when the MTS machine was used. A detailed description of the mechanical test equipment used in these experiments is given by Mellor and Cole (1982).

Acoustic emission equipment

The acoustic emission monitoring system consisted of commercially available equipment. We recorded the number of acoustic events throughout each of the tests as a function of time. In most tests, two transducers were used on each sample (see Fig. 1). Each transducer was connected to a separate acoustic emission monitoring and recording system. The two systems were set at different sensitivities so that some information on the amplitude distribution of the acoustic events could be gained.

The transducers and mountings were modified to obtain the best results possible without interfering with the deforming specimen. The face of each transducer was machined to the same radius as the ice specimens (25.4 mm). Each transducer was fitted into a spring-loaded mounting that pressed the transducer against the specimen with a force between 0.58 and 2.7 N, depending on the extent to which the spring in the mounting was compressed. To acoustically couple the transducer to the specimen, a thin layer (about 0.1 mm) of silicon-based high vacuum grease was placed between the transducer and the specimen. Holes were cut into the membrane surrounding the specimen so that the transducer could be brought into direct contact with it. Skirts made of the same latex membrane material were attached to the transducers with O-rings and sealed to the membrane with heavy grease to prevent material loss around the transducers. With this transducer arrangement, lateral strains could be accommodated and sublimation prevented during long-term tests.

The signal from the transducer was preamplified by 60 dB and band-pass filtered. The -3 dB points for the high-pass and low-pass filters were set between 110 and 510 kHz for the high-gain system (88 dB) and between 105 kHz and 300 kHz for the low-gain system (66 dB). After preamplification and filtering, the signal was processed through a post-amplifier and event counter.

The two acoustic emission systems were operated at different levels of sensitivity. The high sensitivity system was operated at a total amplification of 88 dB and the low sensitivity system was operated at 66 dB. The decibel gains correspond to numerical gains of 2.63×10^7 and 1.64×10^3, respectively.

The threshold level at which events are detected is set so that electronic and mechanical noise does not trigger the event counter when the sample is not loaded. As a matter of expediency, this value is taken as twice the level at which counts are recorded without load application. Typically, the threshold values for the high sensitivity setting (88 dB) was 1.14 V. The threshold value for the low-sensitivity system (66 dB) was 0.8 V. These threshold values indicate that, for an event to be counted, the electric signal at the output of the transducer had to exceed 43 μV for the high gain system and 402 μV for the lower gain system.

If any amplified signal exceeded the present threshold level, it was counted as an acoustic event. When the time between successive threshold crossings was less than 150 μs, then the incoming signals were processed together as a single event. When the time between threshold crossings (dead time) exceeded 150 μs, each crossing was counted separately. (The 150-μs event discrimination time is a parameter determined by the manufacturer.) For our application, this time is approximately one-tenth the duration of a typical acoustic event, and except in certain cases of high loads, the acoustic events often occur several milliseconds apart.

The transducers used in this work were commercially available acoustic emission products with peak sensitivity at 175 kHz. The calibration data accompanying the transducer, from the manufacturer, present the sensitivity in terms of dB referenced to volts per microbar as a function of frequency. If we assume that the transducer is excited at its peak sensitivity, an estimate of the strength of the stress wave impinging on the transducer face can be obtained. Although the absolute units of calibration may not be correct (Dunegan/Endevco 1979), the sensitivities of transducers when compared to each other are self-consistent.

For the high gain system, the transducers had a maximum sensitivity of -70 dB referenced to 1V μbar^{-1} at 175 kHz. The lower gain system has a sensitivity of -73.6 dB referenced to 1V μbar^{-1} at the same frequency. To obtain the sensitivity of the transducer in terms of electrical output per unit of stress, (gauge factor) we apply the formula

$$E_o = E_R \, 10^{(dB/20)} \qquad (1)$$

where E_o is the output sensitivity, E_R is the reference sensitivity in volts per pascal and dB is the output of the transducer. For the transducer which has a maximum sensitivity of -70 dB, the value is 3.16×10^{-3} V Pa^{-1} and for the -73-dB transducer, the corresponding gauge factor is 2.24×10^{-3} V Pa^{-1}.

From the above gauge factors we can consider the relative sensitivity of the high and low gain systems in reference to the threshold sensitivity of each. Thus for the high sensitivity system (which counts events above 43 μV) the nominal pressure threshold is 13.6×10^{-3} Pa (43×10^{-6} V/3.16×10^{-3} V Pa^{-1}) and for the low sensitivity system (which counts events when the transducer output is greater than 402 μV) the nominal pressure threshold is 0.18 Pa (402×10^{-6} V/2.24×10^{-3} V Pa^{-1}). In terms of the relative sensitivities of the two systems employed, we calculate that the high gain system has 14 times the sensitivity of the lower gain system.

For most of the data recorded, the threshold and gain setting levels are typical of those indicated above.

Data recording

In all instances the data were recorded in terms of the total number of acoustic events vs time; this record was differentiated numerically to obtain the event rate. In manipulating and displaying the acoustic data, we have assumed that the acoustic emissions are best characterized by normalizing them to the volume of the specimen. To obtain the total number of events recorded for any of the data presented, multiply by the volume of the ice sample, which is 2.574×10^{-4} m^3.

In calculating the stress values, we have assumed that the material is incompressible (i.e. Poisson's ratio is 0.5). This is a poor approximation for low strains and a relatively good approximation for larger strains (greater than 1%).

ACOUSTIC EMISSION SOURCES IN ICE

Acoustic events and visible fracturing

In many materials the source of acoustic emissions is not understood or is assumed to be a given mechanism based on the best available information. In ice, at least one of the sources of acoustic emissions is clearly associated with the development of cracks. On a large scale, such as the calving of ice blocks from glacier tongues or the propagation of a crack in lake ice, the correlation of the acoustic and visual phenomena of fracture leaves little reasonable doubt as to the source of the acoustic emission. Even as the scale of the fracture event is decreased (as with, for example, the thermally induced fracture of an ice cube in a warm fluid) the correlation between the audible report and the visual observation of fracture is striking. However, as the size of the fracture decreases or the number of fractures per unit volume increases, the source of acoustic emissions becomes less obvious.

Both Gold (1960) and Zaretsky et al. (1979) have assumed that there is one-to-one correspondence between acoustic emissions and fractures in ice. This appears to be the correct assumption when the stress levels are such that visible cracks are produced. In our experiments, however, we often recorded acoustic activity where no visible cracks were observed, particularly during our low load experiments (below ≈ 2 MPa). We noted that the amplitude of these emissions was considerably lower than the amplitude associated with visible fractures.

Source mechanisms

Wakahama (1964, 1965) made an extensive microscopic investigation of the deformation and fracture of polycrystalline ice. His observations were made on thin sections (10x 30x 1 mm) of ice as they were deformed. In ice samples deformed at a temperature of -5°C and at compressive strain rates near 3×10^{-5} s^{-1}, he observed both intergranular and intragranular fractures, which he attributed to a number of different mechanisms.

The intragranular fractures Wakahama (1965) observed consisted of triangular nucleus fractures, transgranular fractures that originated from grain boundaries, and cleavage fractures that propagate primarily along the basal plane. He also observed

intergranular fractures that traversed several ice grains and were exhibited as a visible fracture.

A likely source of low energy acoustic emissions (microfractures) in ice is the formation of small intracrystalline fractures due to crack propagation from low-angle grain boundaries which are formed at low strains. To explain this type of fracture, Wakahama considers the generation of large tensile stresses resulting from the pileup and subsequent breakaway of dislocations at low angle boundaries.

At low deformation rates (and correspondingly low stresses) Wakahama (1964) notes the formation of bend planes in individual grains of the ice matrix. These bend planes are observed under polarized light as isochromatic bands. If the stress is low enough, no fracture will result. However, if the rate of straining is sufficiently high, small triangular fractures nucleate perpendicularly to the bend planes.

Wakahama (1965) postulates that the bend plane fractures are formed as the result of the pileup of dislocations. He also presents an equation to estimate the intensity of the tensile stress at the tip of the pileup.

Presumably, if the rate of stress application is low enough, dislocations will diffuse away from the tips of the dislocation pileups, and the length of the pileup will never become so great that a stress fracture develops. On the other hand, if the load rate is sufficiently high, causing dislocations to pile up faster than they can diffuse away, stresses will increase and a fracture will eventually occur.

In addition to this type of intragranular fracture, Wakahama (1965) also observed fractures that originate at grain boundaries and propagate through the ice grain. A third type of intragranular fracture observed was cleavage fracture, which propagated intermittently along the basal plane. Relative to our investigation, the intragranular fracture mechanisms described by Wakahama provide a very plausible source for the low amplitude emissions we recorded.

As the deformation rates and loads on the samples increase, more obvious intergranular fractures and higher amplitude acoustic emissions occur. These fractures have been observed by a number of investigators and have been described for fine-grained polycrystalline ice in detail by both Wakahama (1965) and Hawkes and Mellor (1972). Interestingly, the visual observations made by Hawkes and Mellor are in good agreement with the trends we observe acoustically.

In terms of macroscopic cracks that form in ice subjected to uniaxial compressive loads, Hawkes and Mellor noted that these cracks do not propagate through the specimens. Generally, visible fractures were first observed at strains of 0.1 to 0.3%. The cracks tended to be planar and the frequency of fractures increased with increasing applied stress. As deformation proceeded, the cracks which formed tended to coalesce. Again, we have noted much the same behavior in our experiment.

Figure 2 shows three thin sections of ice specimens used here. Figure 2a is a thin section of a typical undeformed ice sample observed under polarized light. Figure 2b is a thin section of a sample of ice after it was subjected to a constant compressive load of 0.8 MPa and strained to 4.9%. Here relatively few acoustic emissions were detected and no visible cracks were observed. We do note, however, that significant recrystallization has taken place as indicated by the increase in grain size. Figure 2c shows a thin section of a specimen subjected to a compressive load of 3.76 MPa with an axial strain of over 20%. Here, substantial fracturing has effectively reduced the grain size.

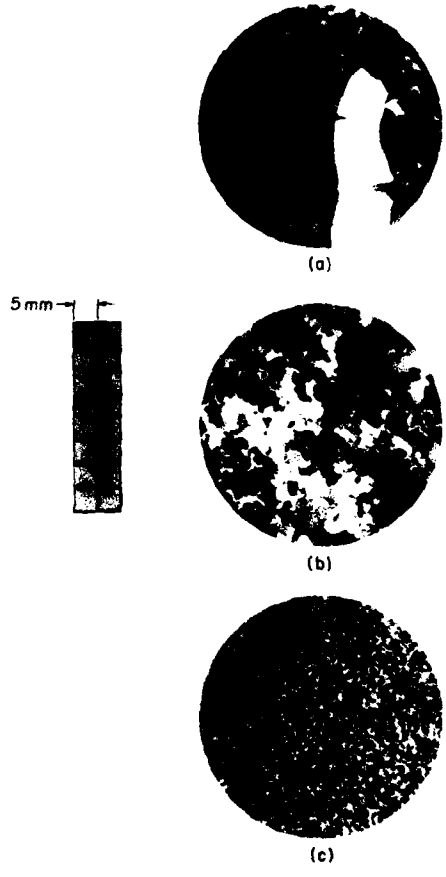

Figure 2. Sections of ice: (a) thin section of an ice sample before testing, (b) thin section of an ice smaple subjected to 1.0-MPa stress and at total strain of 4.9%, (c) thin section of an ice sample subjected to a stress of 3.76 MPa.

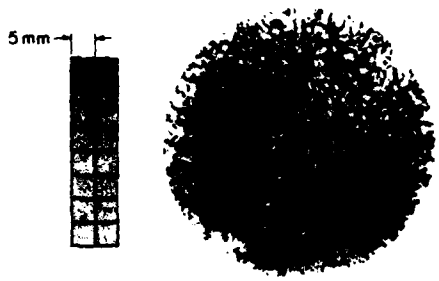

Figure 3. Polished thick section of a specimen subjected to 3.68-MPa stress, T = -10°C. Total axial strain was 6.9%. Cracks have been highlighted with a dye.

In Figure 3 we show a polished thick section of an ice sample that was subjected to a compressive stress of 3.68 MPa with a -10°C test temperature and a 6.9% total axial strain. The dark lines represent coalesced cracks that were formed during deformation. The outlines of the cracks are enhanced for visual observation with a dye. The formation of fractures in the ice specimens is responsible for the dilatant behavior of ice.

Tests on ice single crystals

A brief comparison between the acoustic response of equiaxed polycrystalline ice and ice single crystals will help clarify the role of grain boundaries in the generation of acoustic emissions. In the last section, we associated the source of high and low amplitude emissions with the pileup and subsequent breakaway of dislocations at grain and subgrain boundaries. The results of tests on ice single crystals indicate that, in the absence of grain boundaries, there are no detectable acoustic emissions during deformation.

In these tests for axial stresses of 1 to 2 MPa and a test temperature of -10°C, we found no acoustic emission activity nor visible microfracturing.

In conducting our ice single crystal experiments, the samples were oriented such that the maximum shear stress was on the basal plane of the ice crystal. Also we used a compliant material between the ice and the load platens to avoid stress concentrations. When the compliant material was not used, we found that acoustic emissions were generated. Therefore, we assume that these emissions were generated as a result of stress concentrations at the ice/metal interface.

While we did not observe acoustic emissions with the particular equipment used in our work, the occurrence of acoustic emissions from ice single crystals is not totally precluded. It is very possible that acoustic emissions could be detected in ice single crystals with a more sensitive system, a quieter environment, or operation in a different frequency band. However, for samples in our tests under the same load and temperature conditions, and with the same equipment, we find significant acoustic emission activity in the polycrystalline material, but no measurable activity in single crystal samples.

General acoustic emission response

In examining the acoustic emissions from equiaxed polycrystalline ice, it is clear that the acoustic events recorded are well-behaved in terms of the salient test parameters. Both constant deformation rate tests and constant load tests exhibit total acoustic emission event curves that are smooth, monotonically increasing functions of time. The general forms of the acoustic emission curves are also similar for both constant load and constant deformation rate tests.

The axial strain and the total acoustic events vs time are exhibited in Figure 4. The forms of both the acoustic emission response and the strain response seen in this figure are typical of all the constant load tests performed. For the test shown, the initial applied stress was 2.0 MPa and the sample was strained to over 5%. The strain vs time curve is typical of the constant load tests that were conducted. In this test, the full load was applied at a uniform rate over a time period of 28 s, which is equivalent to a stress rate of 70 $kPa \cdot s^{-1}$. The time of application of the load is short compared to the length of the test.

In Figure 4, the important features of the creep curve are (1) an incubation period that can be identified as an upward facing concavity in the strain vs time curve, (2) a region of constantly decreasing strain rate (primary creep), and (3) a region of increasing strain rate (tertiary creep) which begins at about 3×10^3 s in this particular test. An interesting observation made in all our tests is the absence of any region that can be identified (in a classical sense) as secondary creep, i.e. constant strain rate. Although it is not evident from Figure 4 we noted a brief period without acoustic activity after application of the load. This phenomenon is most likely associated with the development of dislocation pileups and the onset of plastic deformation.

In Figure 4, the acoustic emissions are given as the number of events per unit volume of material. The salient features of the acoustic emission response are (1) a rapid rise in the number of events recorded after application of the load, (2) an abrupt decrease in the rate of acoustic events recorded before the end of primary creep (generally between 0.2% and 0.7%

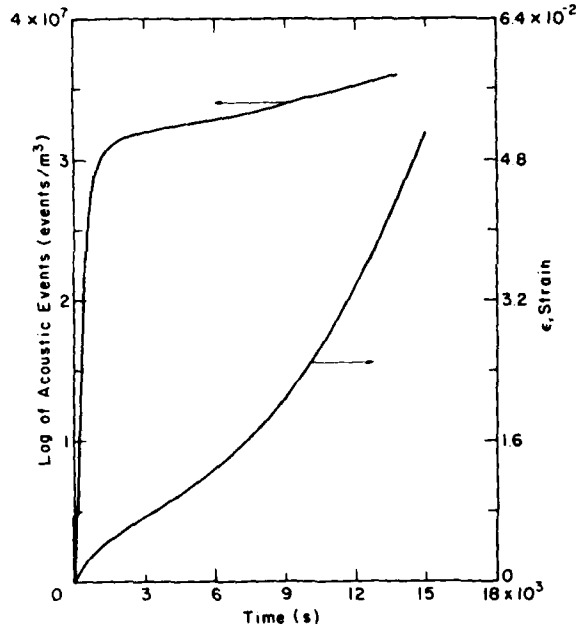

Figure 4. Total acoustic events vs time, and axial strain vs time for an ice speciman subjected to 2.0-MPa stress.

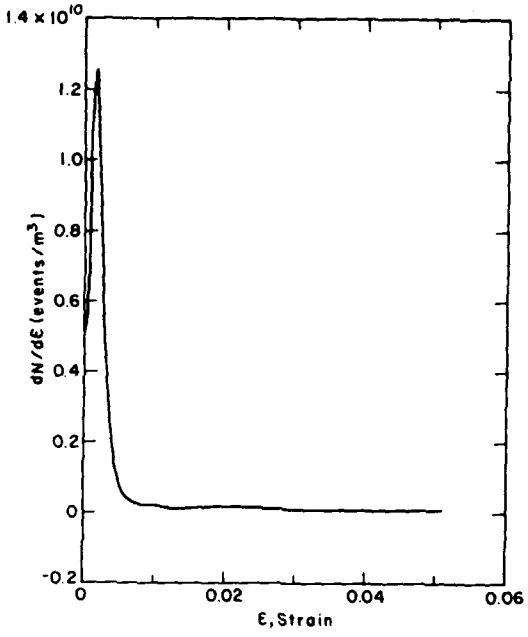

Figure 5. Rate of acoustic emission activity with respect to strain for an ice sample subjected to a constant stress of 2 MPa.

strain), and (3) a relatively constant increase in the number of events as straining proceeds.

The main features of the acoustic emission response can be described with reference to the rate of acoustic activity vs strain presented in Figure 5. As shown, the rate of acoustic activity begins to increase after application of the load. The maximum rate of acoustic activity ($dN/d\epsilon_{max}$) (where N is the number of events and ϵ is the strain) always occurs after the initial maximum of the strain rate and well before the end of primary creep. After the peak in emission activity takes place, the rate drops rapidly. As accelerating (tertiary) creep takes place, the acoustic activity approaches a constant value with respect to strain.

ANALYSIS OF DATA

Transient response

Figure 6 is a graph of the logarithm of the accumulated acoustic activity per unit volume vs strain. The ice samples for this test sequence were subjected to uniaxial compressive loads at -5°C. In these tests, the initial stress values (load divided by original cross-sectional area) ranged from 0.8 to 3.67 MPa. The total number of acoustic events recorded ranged over three orders of magnitude between the lowest and highest stress tests. It can be observed in Figure 6 that the accumulated acoustic emission response is a well-behaved function of stress. Generally the total number of acoustic events at a given strain is greater with increasing stress.

We found that most of the acoustic emissions occurred at strains lower than 0.5% in nearly all tests. Figure 7 is a detailed representation of Figure 6 for strains lower than 1%. It illustrates how rapidly the acoustic activity reaches a nearly steady state when characterized in terms of strain. The initial response is the most difficult to describe quantitatively.

Both Gold (1972) and Zaretsky et al. (1979) have suggested statistically derived distributions to describe the acoustic emission response for columnar grained ice. Gold describes the fracture response in terms of a dual distribution which has the following form:

$$\frac{\partial N}{\partial \epsilon} = 2B\epsilon N_0 e^{-B\epsilon^2} + N_0 e^{-B\epsilon} \qquad (2)$$

where N_0 and B are constants for stress and temperature respectively, and ϵ is the axial strain. Gold* indicates that the first term on the right-hand side of eq 2 is significant for low strain and low stress, and the second term on the right-hand side of the equation

*Personal communication with L.W. Gold, National Research Council of Canada, 1980.

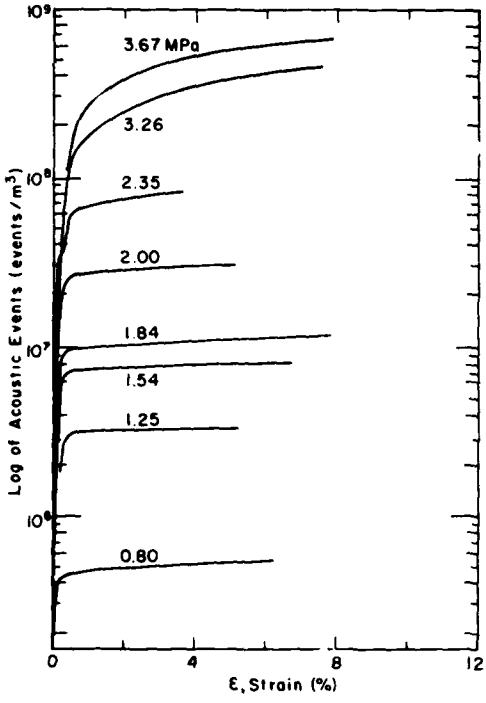

Figure 6. Log-linear plot of the total acoustic activity vs strain for eight test samples subjected to stress from 0.8 to 3.67 MPa. These data correspond to the 88-dB gain system.

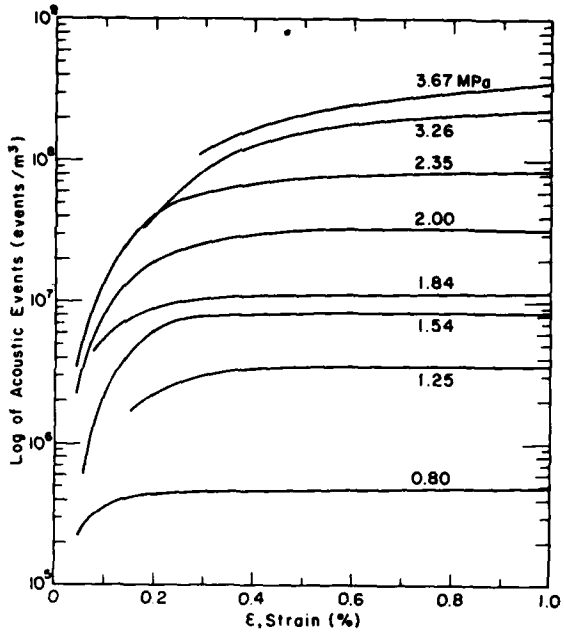

Figure 7. Log-linear plot of the data presented in Figure 6. This graph shows the detail in the acoustic activity versus strain for strains less than 1%.

dominates for higher rates of strain. For constant stress and temperature in eq 2, the partial derivative is identical to the total derivative and upon integration gives:

$$N = N_0 \left(K' - e^{-B\epsilon^2} - \frac{1}{B}\, e^{-B\epsilon}\right) \qquad (3)$$

where K' is a constant which depends on the initial conditions. Equation 3 is appealing since it describes the general form of the total acoustic emission activity. For equiaxed polycrystalline ice the stress threshold at which the second term on the right-hand side of equation 2 becomes important is around 3 MPa.

The equation suggested by Zaretsky et al. (1979) to describe the acoustic emission response is

$$N(t) = N_0 \exp\left[K(T)\left(\frac{\sigma}{\sigma_\infty} - 1\right) t^{1/3}\right] \qquad (4)$$

where $K(T)$ is a function of temperature and σ_∞ is the stress below which no acoustic emissions are detected. For the fine-grained equiaxed ice tested here, we find that eq 4 is limited in terms of approximating the shape of the acoustic emission curve. However, for strains less than 0.5%, it gives a reasonable approximation of the acoustic emission response.

If the strain can be assumed to be proportional to the cube root of time, then eq 4 can be shown to be identical to eq 2, provided that the first term on the right-hand side of eq 2 is small.

As a means of developing a theory for acoustic emissions consistent with current theories of fracture, we favor an equation to describe the *transient portion* of the acoustic emission response based on an analysis similar to that of Stroh (1957). We assume that the fractures causing the acoustic emissions are the result of stresses produced by the pileup and subsequent breakway of dislocations. Stroh (1957) suggests that the probability of fracture can be described in terms of a probability function

$$p = \exp(-t/\tau) \qquad (5)$$

where τ is the mean time elapsing before a dislocation pileup is released, t is the time at which the stress reaches a given value, and p is the probability of

Table 1. Constants A, τ and the corresponding coefficients of determination associated with eq 7.

The constants were determined using a least-squares fit to eq 7 in the form of $\ln [(dN/dt)/N] = \ln A - t/\tau$.

Stress level σ (MPa)	Constant A (events $m^{-3} s^{-1}$)	Relaxation time τ (s)	Coefficient of determination r^2
0.80	3.503×10^{-4}	1.642×10^{3}	0.995
1.25	6.739×10^{-3}	5.105×10^{2}	0.971
1.54	9.515×10^{-3}	3.194×10^{2}	0.957
1.84	1.135×10^{-2}	2.954×10^{2}	0.949
2.00	2.562×10^{-2}	1.781×10^{2}	0.992
2.35	6.228×10^{-2}	9.702×10^{1}	0.991
3.26	7.894×10^{-2}	4.226×10^{1}	0.987
3.67	3.517×10^{-2}	6.693×10^{1}	0.995

fracture. Stroh (1957) suggests that τ in eq 5 be given by the equation

$$\tau = \left(\frac{1}{\nu}\right) \exp \frac{U(\sigma)}{KT} \qquad (6)$$

where ν is a constant with the dimensions of frequency, K is Boltzmann's constant, T is absolute temperature and $U(\sigma)$ is the activation energy needed to free a dislocation.

We can use eq 5 to obtain the acoustic emission intensity per unit time. Since the applied stress σ and temperature are constant, we can use the total derivative to replace p,

$$\frac{dN}{N} = A \exp\left(-\frac{t}{\tau}\right) dt \qquad (7)$$

where A is a constant with the units of frequency. Integrating eq 7 we have

$$\ln N - \ln N_0 = A\tau \left\{\exp\left(-\frac{t_0}{\tau}\right) - \exp\left(-\frac{t}{\tau}\right)\right\} \qquad (8)$$

where N_0 and t_0 represent the lower limits of integration. Taking the antilog of eq 8 yields

$$N = N_0 \exp\left\{A\tau \left[\exp\left(-\frac{t_0}{\tau}\right) - \exp\left(-\frac{t}{\tau}\right)\right]\right\}. \qquad (9)$$

Letting

$$N_0' = N_0 \exp\left\{A\tau \exp\left(-\frac{t_0}{\tau}\right)\right\} \qquad (10)$$

we have

$$N = N_0' \exp\left\{-A\tau \exp\left(-\frac{t}{\tau}\right)\right\} . \qquad (11)$$

When eq 7 and 11 are compared with the corresponding derivative and total acoustic emission data curves we find very good agreement. Qualitatively eq 11, like Gold's distribution equation (eq 2), describes a curve which rises rapidly and approaches the value N_0' asymptotically in a very short time.

Equation 11 is an alternative distribution which serves the purpose of describing the transient portion of the acoustic emission curve. In eq 7 the constant A and the relaxation time τ are empirically determined to obtain a best fit to the test data. Table 1 gives the values of A and τ for the tests in this series and also the corresponding coefficient of determination. Each test is identified by the imposed stress level. The value of N_0' is determined from the steady-state response.

Steady-state response

Generally, we found for most of the tests that the rate of acoustic activity appears to be constant after the specimen is strained beyond approximately 0.5%. For the relatively high stress tests (3.26 and 3.67 MPa) the acoustic rate appears to decrease continuously with increasing strain. However, in terms of an engineering approximation, the data are still relatively well-represented by a constant rate approximation beyond 1% strain. Table 2 presents the coefficients (m, a) obtained by fitting the equation

$$N = m\,\epsilon + a \qquad (12)$$

to the data corresponding to the response curves of Figure 6. In eq 12, N is the number of events per unit volume, ϵ the strain ($\epsilon \geq 0.01$) and a the intercept. Equation 12 is not applicable for strains lower

Table 2. Constants m, a and the coefficient of determination associated with eq 12.

The constants were determined by performing a least-squares fit to the equation $N = m \cdot \epsilon + a$.

Stress level σ (MPa)	Constant m (events m^{-3})	Intercept value a (events m^{-3})	Coefficient of determination r^2
0.80	1.368×10^{6}	4.746×10^{5}	0.948
1.25	4.094×10^{6}	3.386×10^{6}	0.986
1.54	1.538×10^{7}	8.182×10^{6}	0.987
1.84	2.991×10^{7}	1.106×10^{7}	0.997
2.00	1.027×10^{8}	3.159×10^{7}	0.986
2.35	7.194×10^{8}	7.717×10^{7}	0.988
3.26	5.957×10^{9}	1.939×10^{8}	0.974
3.67	8.452×10^{9}	3.185×10^{8}	0.958

than about 0.5%, the point which is considered to be the end of the transient response. Also, although the linear relation of eq 12 has been applied to the test at stress levels of 3.26 MPa and 3.67 MPa, it would appear that we are using the relationship beyond its range of applicability. Special consideration will be given to high stress tests ($\sigma > 3.0$ MPa) later. The linear relationship between axial strain and accumulated acoustic activity has also been noted by Hardy et al. (1970) for other geologic materials. Okajima and Ono (1980) present results which indicate that eq 12 holds for some metals.

From the condition that the slope of the acoustic emission curve is constant with strain, we can examine how the value of the slope m in eq 12 changes as a function of stress (see Fig. 8). A reasonable empirical relation is obtained from

$$m = (5.48 \times 10^5) \exp\left\{1.6369\left(\frac{\sigma-\sigma_\infty}{\sigma_\infty}\right)\right\} . \quad (13)$$

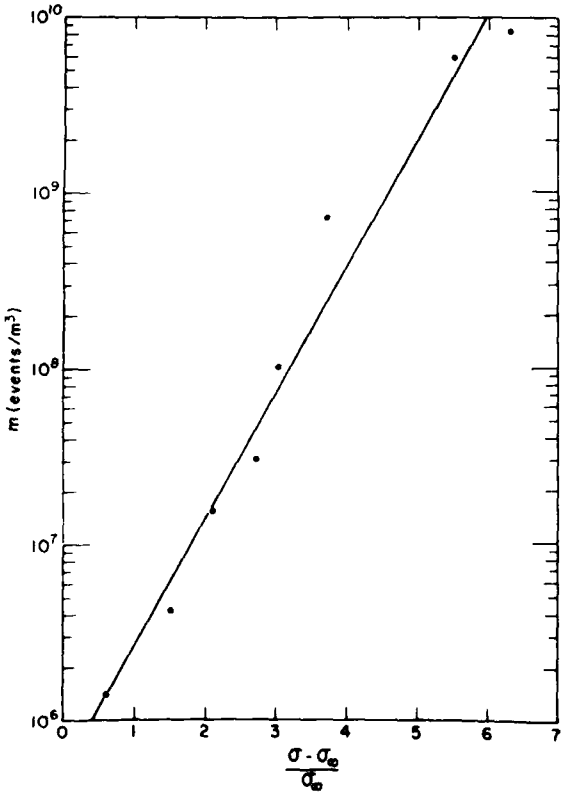

Figure 8. The dependence of the slope m from eq 12 as a function of the nondimensional parameter $(\sigma-\sigma_\infty)/\sigma_\infty$. σ_∞ is taken equal to 0.5 MPa.

In eq 13, σ is in units of MPa and the coefficient has the units of events per cubic meter. The value of σ_∞ is 0.5 MPa, which is the same value used by Zaretsky et al. (1979). The coefficient of determination

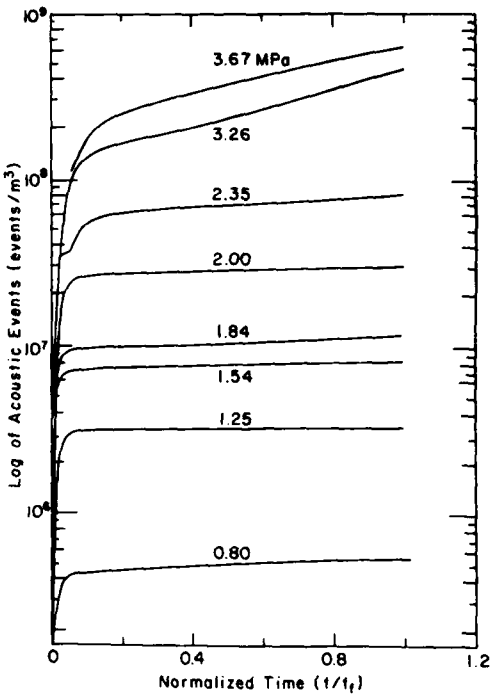

Figure 9. Log of the total acoustic events vs time normalized to the total test time t_f. The value of t_f is given in Table 2.

Table 3. Constants *B*, *K* and the coefficient of determination associated with eq 15.

The constants were determined by performing a least-squares fit to the equation $de/dt = Be + K$. The value of t_f given is the value used to normalize the data for Figures 9 and 12. An asterisk indicates the value of K was taken directly from the data.

Stress level σ *(MPa)*	*Constant* B (s^{-1})	*Intercept value* K (s^{-1})	*Coefficient of determination* r^2	*Test duration* t_f *(s)*
0.80	2.814×10^{-6}	1.114×10^{-7}	0.702	334,800
1.25	2.738×10^{-5}	3.299×10^{-7}	0.941	50,400
1.54	2.569×10^{-5}	4.992×10^{-7}	0.855	41,460
1.84	4.594×10^{-5}	1.261×10^{-6}	0.916	29,400
2.00	1.208×10^{-4}	6.660×10^{-7}	0.979	15,000
2.35	2.884×10^{-4}	4.291×10^{-7}	0.997	7,680
3.26	2.077×10^{-3}	6.635×10^{-6} *	0.982	1,500
3.67	2.436×10^{-3}	1.131×10^{-5} *	0.996	1,080

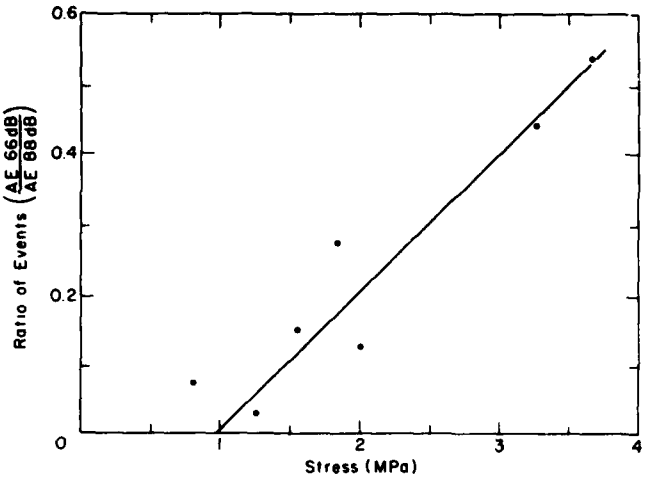

Figure 10. Ratio of the total number of events detected at gain settings of 66 and 88 dB. The points indicate the actual data used and the line is a best fit to the data.

(r^2) for eq 13 fitted to the data of Figure 9 is 0.97. The value of m in eq 13 is also a function of temperature.

Figure 9 is another representation of the data exhibited in Figure 6. In Figure 9 we display the data in terms of the total number of acoustic emissions vs time normalized to t_f, the total test duration for strains between 3.2% and 7.6%. Table 3 lists the values of t_f used to calculate the normalized times plotted in Figure 10. The test data are normalized in this way due to the large variations in the test durations. Each of the curves is identified with the initial stress level of the test.

Amplitude distribution

In many of the tests we monitored the acoustic emission activity at two different amplification levels, generally at 88 dB and 66 dB. By monitoring at these two amplifications we had a rough means of looking at the relative amplitude of emissions throughout each test. An important observation made was that, once the steady-state emission rate was established, the ratio of the amplitudes of the 66- and 88-dB channels remained nearly constant. This indicates that the amplitude distribution of emissions remained nearly constant throughout most of the test. This pattern is different from those observed in rock (Shultz 1968) in which the amplitude of emissions tends to increase as the specimen progresses toward failure.

Another notable feature became evident in examining the ratio of the acoustic emission amplitudes. As the applied stress increased, the ratio of higher amplitude emissions (66 dB) to the total number of emissions increased. This relationship indicates that the size of the acoustic source, and therefore the amplitude of the acoustic emission, generally increases with stress. Figure 10 shows the change in the ratio of high and low amplitude emissions for various stresses. Although the data are scattered, a definite trend is apparent. In characterizing these data, we found that a linear relationship provided the best fit. Figure 10 shows the best straight line fit to the data in the applied stress interval from 0.8 to 3.67 MPa. The regression equation fitted to these data is

$$\frac{N_{66dB}}{N_{88dB}} = -0.1262 + 0.1748\sigma \qquad (14)$$

where σ is in megapascals. The coefficient of determination (r^2) associated with this curve is 0.94.

COMBINED TRANSIENT AND STEADY-STATE RESPONSE IN THE TIME DOMAIN

We have described the acoustic emission response in terms of a transient response in the time domain and a steady-state response in the strain domain. We can combine the overall response of the acoustic emission activity (transient and steady state) by noting that the strain rate in the tertiary part of the creep curve can be reasonably approximated by considering it to be proportional to the strain. This response is described by the equation

$$\frac{d\epsilon}{dt} = B\epsilon + K \qquad (15)$$

for stresses greater than 0.8 MPa and for strains greater than 0.85%. In eq 15 B is a constant, ϵ is the axial strain, K is an intercept value and $d\epsilon/dt$ is the strain rate. Figure 11 illustrates this relation for an ice specimen subjected to a constant stress of 2 MPa. The straight line in the figure represents a least-squares fit to the experimental data points for strains between 0.88 and 5.1%. The coefficient of determination (r^2) for this curve is 0.98. It is important to note that the linear relationship expressed by eq 15 breaks down for strains greater than about 5% for all tests conducted to date. Over the range of stresses applied in this series of tests, we found that the strain

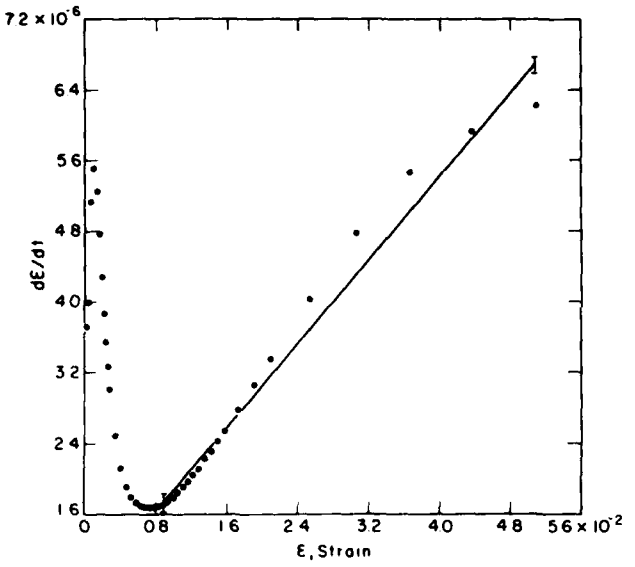

Figure 11. Strain rate vs strain for an ice sample subjected to a stress of 2 MPa. The data points are taken from the test data. The straight line in the figure is a least-squares fit to the data between strains of 0.88% and 5.2%.

rate tends to increase at a reduced rate at strains over 5%. We attribute this to syntectonic recrystallization and the fact that these tests were at constant load rather than constant stress. The values of B, K and r^2 from eq 15 for each test are given in Table 3.

Recall that we described the acoustic emission activity in the steady state phase with respect to strain by

$$N = m\,\epsilon + a \tag{12}$$

noting that

$$\frac{dN}{d\epsilon} = m\,. \tag{16}$$

Applying the chain rule, we have

$$\frac{dN}{dt} = m(B\epsilon + K)\,. \tag{17}$$

By solving eq 12 for ϵ, substituting in eq 17 and rearranging, we obtain the differential equation

$$\frac{dN}{dt} - BN = (mK - Ba)\,. \tag{18}$$

Using the initial condition that $N = a$ at time $t = 0$, we obtain the solution to eq 18:

$$N = a + \frac{mK}{B}\,(e^{Bt} - 1)\,. \tag{19}$$

To review, the constants a and m are from the acoustic emission response curve (eq 12) and the constants B and K are obtained from the strain rate curve (eq 15). Equation 19 indicates that we should observe an exponential increase in the number of acoustic emissions with time in the region of applicability. This region occurs after the initial rapid rise in the acoustic emission curve.

However, by considering eq 19 more closely, we can use it to approximate the total acoustic emission response in the time domain. We can do this by noting that the value of a is much greater than the value of mK/B and also that for small times the value of $[\exp(Bt) - 1]$ in eq 19 is very near zero. So, during the rapidly rising transient portion of the acoustic emission curve, the second term on the right-hand side of eq 19 is small when compared to the quantity a. Noting this we let

$$a = N_0' \exp(-A\tau e^{-t/\tau}) \tag{20}$$

by letting $a = N$ in eq 11. We also note that the exponential term in eq 20 rapidly approaches asymptotically the value of one as t increases. Therefore in the limit

$$a = N_0'\,. \tag{21}$$

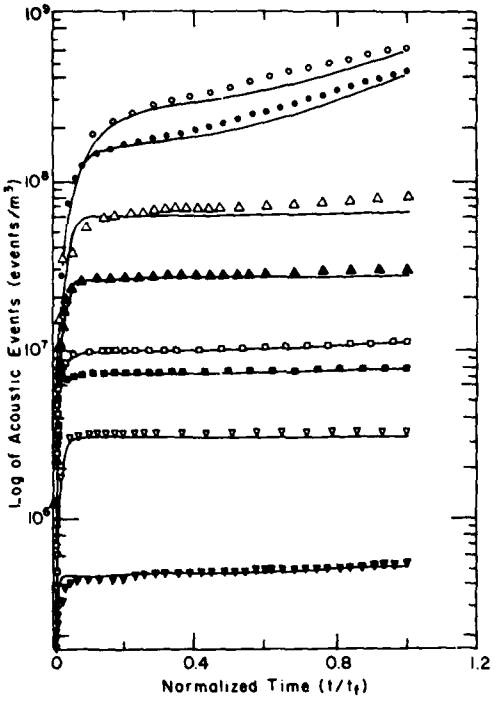

Figure 12. Log-linear plot of the actual acoustic response and that predicted from eq 21. The data are represented by points and the solid lines are the values determined from eq 21.

Considering these facts we can approximate the total acoustic emission response with respect to time by the equation

$$N = N_0' \exp\left(-A\tau e^{-t/\tau}\right) + \frac{mK}{B}\left[\exp\left(Bt\right) - 1\right] \tag{22}$$

We note that eq 22 does not hold for the small times at the beginning of the test where the terms on the right-hand side of eq 22 are close to the same value.

Figure 12 is a log-linear plot of the total acoustic events vs time normalized to the final time of the test. The data points and the calculated values of the acoustic emissions for eq 22 are shown. The values of the constants in eq 22 are taken from Tables 1-3. Equation 22 represents the data well over three orders of magnitude. The time range at which each of the two terms in eq 22 dominates can be seen in Figure 12. During the rapid rise in the acoustic activity, for $t/t_f < 0.05$, the first term in eq 22 dominates. As the acoustic activity levels off for $t/t_f > 0.05$, the second term on the right-hand side of eq 22 dominates.

Table 4. Values of the constants a', n and the coefficient of determination associated with eq 23.

The constants were determined by performing a least-squares fit to eq 23 in the form $\ln N' = \ln a' + n \ln \epsilon$. The strain ($\epsilon$) is the lowest strain limit for which eq 23 applies.

Stress level σ (MPa)	Constant) a' (events m^3)	Exponent n	Coefficient of determination r^2	Lower strain limit ϵ_0
3.26	2.2628×10^9	0.5011	0.998	0.004
3.67	3.1763×10^9	0.4786	0.998	0.008

In order to use a consistent representation of the data in all our experiments, the steady-state values were determined in the forms of eq 12 and 15. These equations produced a reasonable fit to the data for all values of stress. However, in considering the very high stress tests ($\sigma > 3$ MPa) some changes in the mechanism of deformation take place due to the significant amount of fracturing, as can be observed in Figure 3. In each of these cases the intercept value (K) in eq 15 is negative. For the purpose of evaluating the acoustic emission response from eq 22 we have determined the intercept value (K) from the acoustic emission data.

We have also used the linear equation (eq 12) to represent the acoustic emission response in the case of the high stress tests ($\sigma = 3.26$ MPa and $\sigma = 3.67$ MPa). The representation of these data is acceptable, with coefficients of determination of 0.974 and 0.958 for stresses of 3.26 MPa and 3.67 MPa respectively. However, for these two particular tests, an equation of the form

$$N = a' \epsilon^n \tag{23}$$

may be more appropriate than eq 12 since the negative k value is avoided. Table 4 gives the values of a' and n along with the coefficient of determination in each test. ϵ_0 in Table 4 is the minimum strain for which eq 23 applies. For both tests the exponent n is about 1/2. Although eq 23 produces a better fit to the data for high stresses, it complicates the solution of the differential equation in the time domain. For this reason we feel that the less accurate, but more convenient, representation given by eq 12 can be used.

DISCUSSION

The detection of acoustic emissions is an excellent indicator that deformation is being accommodated

by local fracture. Thus the acoustic emission activity can be used to delineate the region of dislocation creep with cracking (Shoji and Higashi 1977). Since we have not detected acoustic emissions in ice single crystals (at comparable levels of equipment sensitivity) we suspect that the fractures we observe are closely related to the presence of grain boundaries. This concept is in accord with work in the literature.

In quantitatively describing the data we considered the response to be composed of two phases: a rapidly rising transient portion and a slowly increasing secondary phase. To explain these responses we make the assumption that the acoustic emissions result from fractures associated with the breakaway of dislocation pileups. This explanation allows us to apply a theory analogous to that proposed by Stroh (1957) in order to develop a time-dependent term for the transient portion of the acoustic emission curve. The secondary part of the curve can be described either in terms of time or strain. The primary and secondary portions are combined to describe the total acoustic emission response in the time domain.

In developing the equations to describe the acoustic emission response, we relate the acoustic events to the deformation of the specimen. For the tertiary portion of the strain vs time curve we observe that the strain rate is proportional to the strain. We find this to be true for all the stress levels we tested from 0.8 to 3.67 MPa. However, this relationship breaks down significantly after strains near or greater than 5%. We attribute this primarily to recrystallization of the ice. Thin-section analysis shows a consistent decrease in the grain size of the ice samples after testing for stress levels greater than about 3.26 MPa. Here, the grains tend to be broken by large fractures. For stresses below about 2.35 MPa, noticeable grain growth occurs. Considerably fewer high energy emissions are produced at these low stress and recrystallization mechanisms such as grain boundary migration are able to operate.

The acoustic emissions appear to be a consequence of the flow process, and a fracture, once initiated, acts as a sink for dislocations. This leads to the observed behavior $N \approx \epsilon$. It should be noted that for stresses above 3 MPa the relationship between strain and bursts of acoustic energy is better represented by a relation $\epsilon \approx N^2$. However, for our initial approximation we have used a linear form for simplicity.

In general, we find that observations of the acoustic emissions are important in describing the formation of microfractures in ice, and are especially important in discussions of the deformation at high stress.

SUMMARY

In this work we have reported the results of an investigation of acoustic emissions from equiaxed polycrystalline ice. Constant load creep tests were performed on polycrystalline ice with equiaxed grains of 1.2-mm diameter. Applied loads varied from 0.8 to 3.67 MPa; test temperature was -5°C.

The acoustic emissions were monitored by two transducers in contact with the specimen. Separate signal processing systems allowed us to record events at two gain levels, giving an indication of the amplitude distribution of the events.

Generally, a short incubation time with little acoustic activity followed specimen loading. A dramatic rise in the acoustic emission rate then occurred, tapering off between 0.3 and 0.5% axial strain. Ninety percent of the total number of acoustic events in the test occurred during this transient phase. A steady-state condition followed at strains over 0.5% in which the acoustic emission rate was fairly constant and much lower than in the transient phase. The acoustic response was closely related to specimen strain and the basic trends did not vary significantly from specimen to specimen.

Source mechanisms were also considered. The use of two monitoring systems set at gain levels of 66 and 88 dB allowed us to characterize the emissions as either of high amplitude associated with visible fracture or of low amplitude with no visible fracturing. In either case, the acoustic events are assumed to result from the breakaway of dislocation pileups. Work by Wakahama (1964 and 1965) was relied upon to assess probable sources of acoustic emissions.

Intergranular fractures were assumed to generate the high amplitude emissions occurring at higher stresses ($\sigma > 2.5$ MPa). At lower stresses (and correspondingly lower strain rates), when the dislocations could presumably diffuse away from the pileups, visible fracture would not occur.

In the stress range of 0.8 to 2.5 MPa, where visible fracturing did not occur, a significant number of low amplitude acoustic events were nonetheless recorded. These were assumed to be generated by small intragranular cracks.

A close connection between the occurrence of detectable acoustic emissions and the presence of grain boundaries was implied by the explanations of the source mechanisms. To reinforce this implication, we conducted several constant load experiments on ice single crystals. No acoustic emissions were detected with loading conditions and instrument sensitivities similar to those in the polycrystalline ice tests. This clearly indicated that grain and subgrain boundaries play a significant role in the generation of detectable acoustic emissions.

An expression for the total number of acoustic events was developed. The acoustic response was divided into two segments for this purpose: an initial

transient phase ($\epsilon < 0.005$) and a steady-state phase ($\epsilon > 0.005$). The expression for the transient phase was modeled after a probability function giv by Stroh (1957). The steady-state phase was represented by a simple linear model. The constants in both expressions were determined from the test data and were primarily functions of stress (temperature and grain size were not varied in these tests). A linear approximation in the steady-state response expression limits the useful range of the expression to less than 5.0% axial strain.

LITERATURE CITED

Brown, E. (1926) Experiments on the strength of ice, St. Lawrence Waterway Project. Report, Joint Board of Engineering, App. F., Ottawa.

Cole, D.M. (1979) Preparation of polycrystalline ice specimens for laboratory experiments. *Cold Regions Science and Technology*, vol. VI, p. 153–159.

Dunegan/Endevco (1979) An absolute impulsive surface wave transducer calibration. *Now Hear This*, (a newsletter on acoustic emission), Dunegan/Endevco Corp., San Juan Capistrano, California, September.

Gavrilo, V.P., A.V. Gusev, Y.K. Zaretskiy, and A.M. Fish (1979) Acoustic emission as an indicator of the process of deformation and break-up of ice. In *Physical characteristics of geophysical processes in polar regions.* CRREL Draft Translation 702, p. 59–68.

Gold, L.W. (1960) The cracking activity in ice during creep. *Canadian Journal of Physics*, vol. 38, no. 9, p. 1137–1148.

Gold, L.W. (1972a) The failure process in columnar-grained ice. National Research Council of Canada. Report 12637, p. 108.

Gold, L.W. (1972b) The process of failure of columnar-grained ice. *Philosphical Magazine*, vol. 26, no. 2, p. 311–328.

Hardy, H.R., R.Y. Kim, R. Stefanko and Y.J. Wang (1970) Creep and microseismic activity in geological materials. *Rock Mechanics—Theory and Practice, Proceedings of the Eleventh Symposium on Rock Mechanics*, Berkeley, American Institute of Mechanical Engineers, p. 377–413.

Hawkes, I. and M. Mellor (1972) Deformation and fracture of ice under unaxial stress. *Journal of Glaciology*, vol. 11, no. 61, p. 103–131.

Mellor, M. and D.M. Cole (1982) Deformation and failure of ice under constant stress or constant strain rates. *Cold Regions Science and Technology*, vol. 5, p. 201–219.

Okajima, K. and K. Ono (1980) Temperature dependence of anisotropic AE behavior of A533B Steel. Technical Report No. 80-03, Office of Naval Research, Contract No. N00014-75-C-0419.

Shoji, H. and A. Higashi (1978) A deformation mechanism map of ice. *Journal of Glaciology*, vol. 21, no. 85, p. 419–429.

Shultz, C.H. (1968) Mechanism of creep in brittle rock. *Journal of Geophysical Research*, vol. 73, p. 3295–3302.

Stroh, A.N. (1957) A theory of the fracture of metals. *Advances in Physics*, vol. 6, p. 418–465.

Wakahama, G. (1964) On the plastic deformation of ice. V. Plastic deformation of polycrystalline ice. *Low Temperature Science*, Japan, Ser. A2, p. 4–23.

Wakahama, G. (1965) Internal fracture of ice. *Low Temperature Science*, Japan, Ser. A23, p. 41–49.

Zaretsky, Y.K., A.M. Fish, V.P. Gavrilo, and A.V. Gusev (1976) Short-term ice creep and microcrack formation kinetics. CRREL Draft Translation 539, p. 196–202.

Zaretsky, Y.K., B.D. Chumichev and V.I. Solomatin (1979) Ice behavior under load. *Engineering Geology*, vol. 13, p. 299–309.

A facsimile catalog card in Library of Congress MARC format is reproduced below.

St. Lawrence, William F.
Acoustic emissions from polycrystalline ice / by William F. St. Lawrence and David M. Cole. Hanover, N.H.: U.S. Cold Regions Research and Engineering Laboratory; Springfield, Va.: available from National Technical Information Service, 1982.
iv, 26 p., illus.; 28 cm. (CRREL Report 82-21.)
Bibliography: p. 15.
1. Acoustic emission. 2. Ice. 3. Mechanical properties. 4. Polycrystalline ice. I. Cole, David M. II. United States. Army. Corps of Engineers. III. Army Cold Regions Research and Engineering Laboratory, Hanover, N.H. IV. Series: CRREL Report 82-21.

☆U.S. GOVERNMENT PRINTING OFFICE: 1982 – A-2294/171

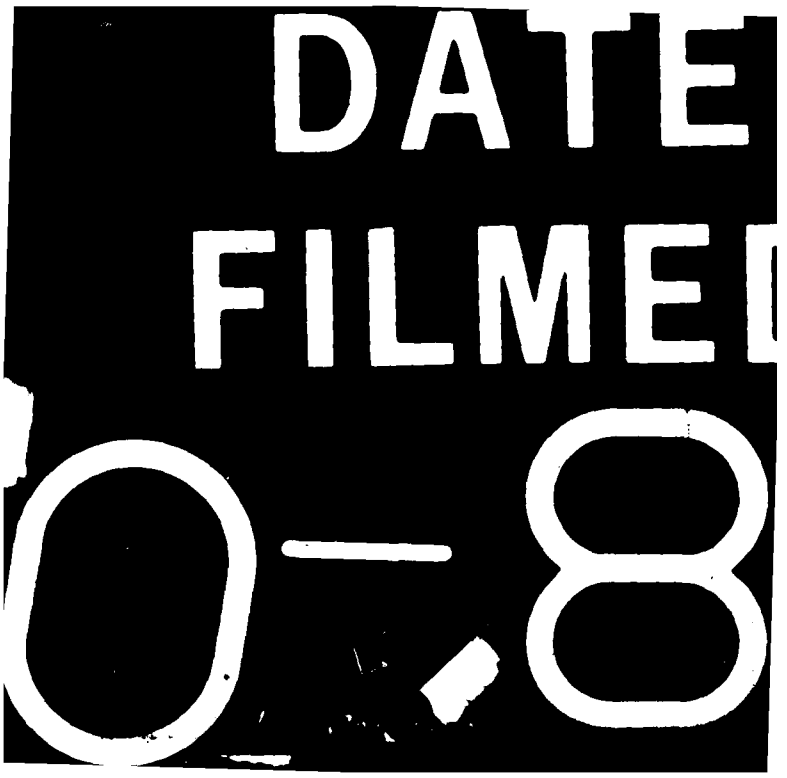
DATE
FILME
0-8